CHAPTER IV

RESULT AND DISCUSSION

In this research, the combined finite element and moment method is applied to calculate the electric field distribution of edge slot antenna that works on the X-frequency band for the numerical examples. The characteristic of edge slot antenna such as admittance parameters and radiation pattern is calculated from this field distribution. The numerical performance is evaluated by comparing the results to other methods and some measurement data taken from published paper. The result of the numerical calculation and its evaluations are presented in this following chapter.

4.1 Electric Field Distribution

Initially, the combined method with common element shape function is used to calculate the electric field distribution along the edge slot. The first numerical example is done for the edge slot antenna that cut on a standard X-band waveguide (width 0.9 inches, height 0.4 inches and wall-thickness 0.05 inches) and operated at 9.375 GHz. The slot has dimension of inclination angle $\theta = 15°$ and width $w = 0.0625$ inches. The extended part of slot in the bottom and top wall of waveguide is 0.14 inches.

The method is applied by dividing the cavity region into two layers and 64 triangular elements in each layer. The calculation result is depicted in Fig. 4.1 and Fig. 4.2. The distribution of electric field along the slot is found closed to sinusoidal that has maximum on the center and vanishes on both ends. The phase is nearly constant with a bit discrepancy for slot part on the broad-wall. The fields on center line, inner, and outer surfaces have some discrepancy that is caused by the wall-thickness. The presence of the slot corners affects to the electric field distribution which deviates unsmoothly around the corners especially on the outer

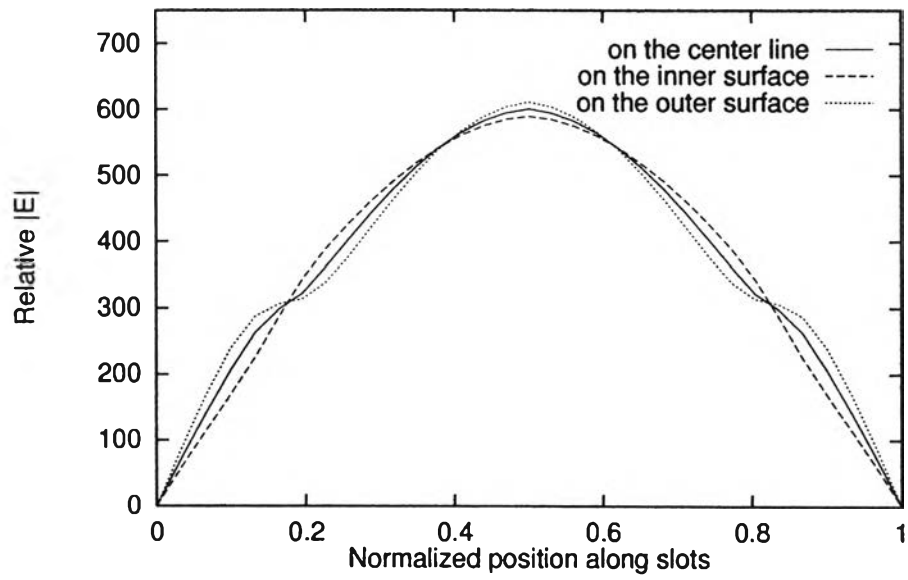

Figure 4.1: Magnitude of electric field on inner, center and outer slot surface for the first case.

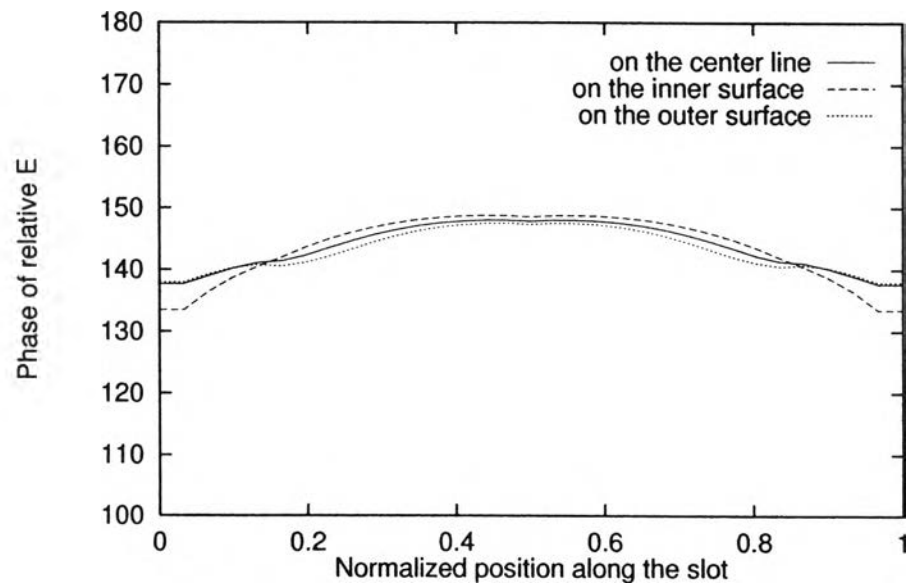

Figure 4.2: Phase of electric field on the inner, center and outer slot surface for the first case.

surface. This is possibly caused by the assumption of the electric field direction and the formulation of corner effect that are slightly invalid.

The theory of slot antenna states that it has similar characteristic with the half dipole antenna, so that the distribution of electric field is approximately sinusoidal along the slot length. Therefore, the calculation result is agree with this theory. It is also agree with the assumption in the Stevenson's work.

4.2 Evaluation of Numerical Convergency

The number of elements on the analysis is needed to be adjusted to any number of element in which the calculation gets the appropriate result or convergence condition. In order to know the required number of elements, the analysis is run on various number of layer and elements.

To evaluate the convergence, it is taken the calculation result for the nodes on the external slot corner and center of slot on the external surfaces. This choice of these nodes is considered that they have the same coordinates although we change the number of either layer or element. It also regards that the field always reach the maximum value on the center and the field also tends to variate more rapidly on the corners due to its singular characteristics.

The calculation result that is depicted in Fig. 4.3 shows that calculation results of both peak and corner value are almost similar for two and three layer, but it has significant discrepancies with the one layer. It means that we need at least two layer to get the appropriate results.

The variation of element in each layer yields the results that are nearly constant for the number of element more than 44 elements per layer. The large differences of one layer calculation are also possibly influenced by the shape of element that possibly becomes improper triangular shape if the number of element is not suitable with the number of layer. The reason is the dimension of element along the wall thickness is not changed when the number of element is increased without changing the layer number.

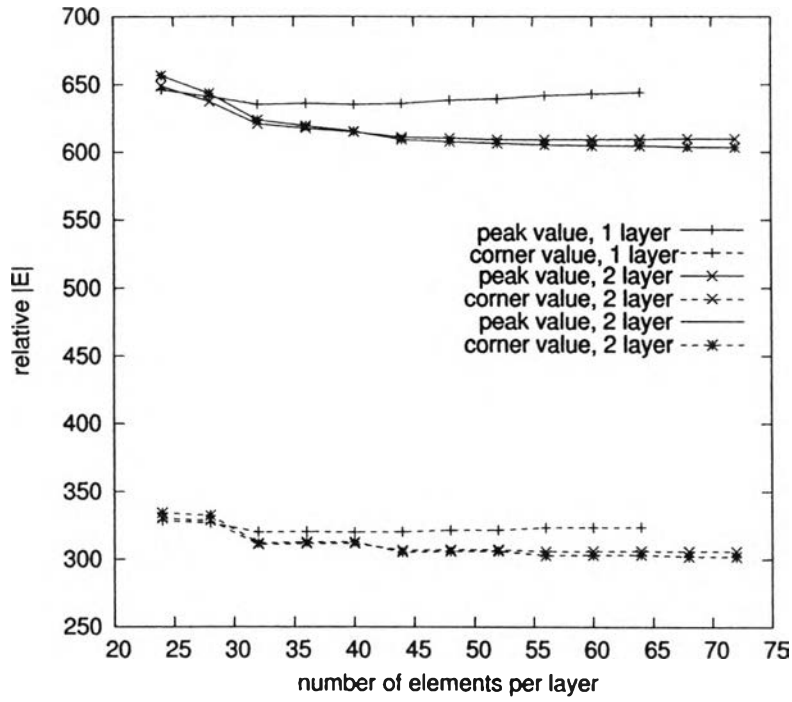

Figure 4.3: The comparison of calculation result with various number of layer and element.

According to the result of convergency test, it is chosen two layer and 64 element per layer for further calculations that work on the same frequency range and waveguide dimensions.

4.3 Singular Element Implementation

One of the contribution proposed in this thesis is the application of the singular element shape function to improve the accuracy and convergence of the analysis especially on the corner. To evaluate its performance, the same slot as in the section 3.1 is analyzed using combined FEM/MoM with singular element shape function. To choose a suitable value of quadratic parameter ρ, it is done by trying for any number of ρ, and the results are shown in Fig. 4.4 to 4.7.

The results on those figures show that the electric field distributions on both inner and outer surfaces are similar to the standard element for $\rho = 0$, but the magnitudes are increased and the arguments are decreased for the nonzero of ρ.

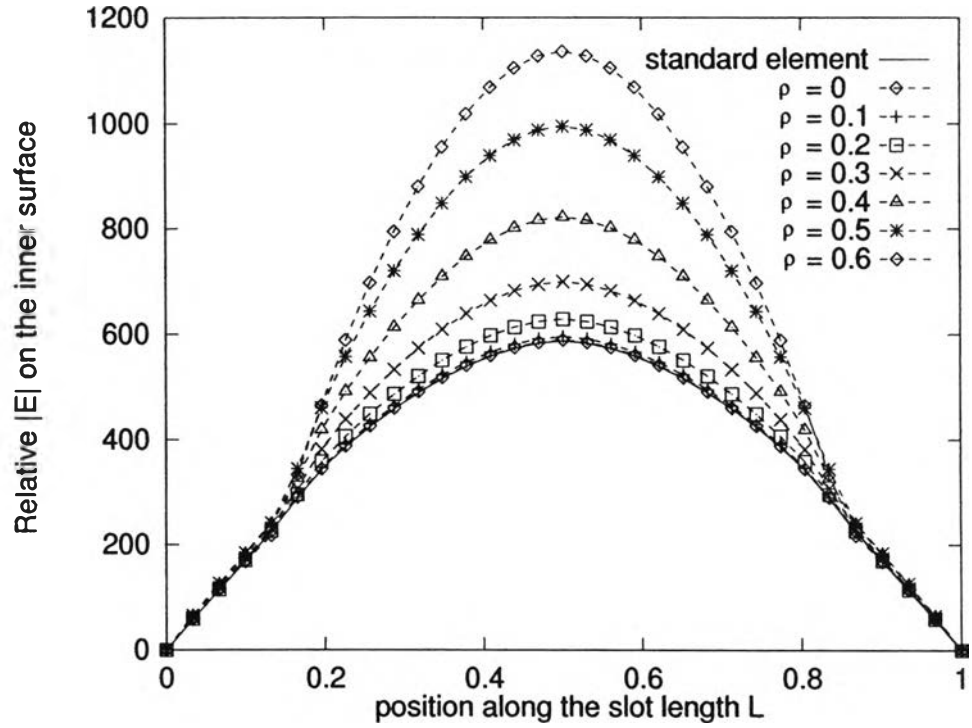

Figure 4.4: The magnitude of electric field along the inner surface for various number of ρ

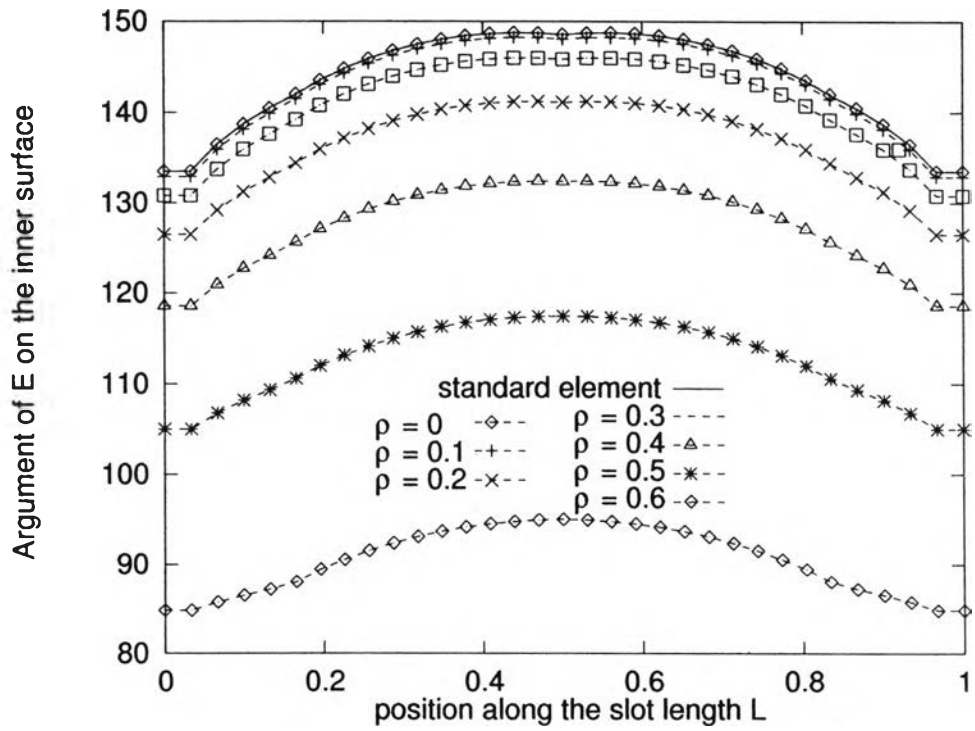

Figure 4.5: The argument of electric field along the inner surface for various number of ρ

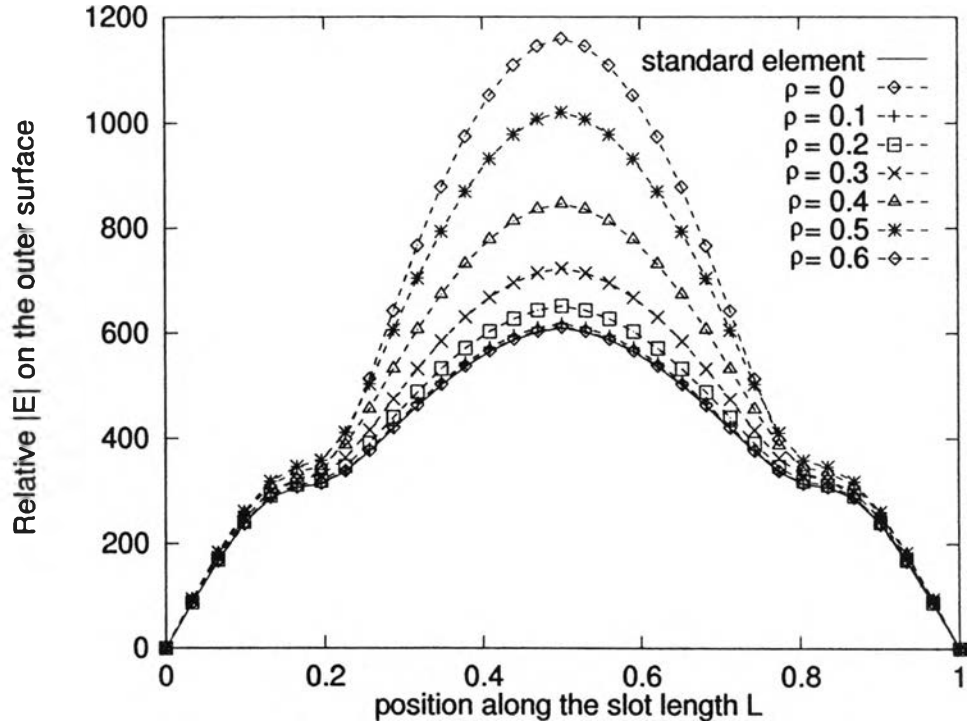

Figure 4.6: The magnitude of electric field along the outer surface for various number of ρ

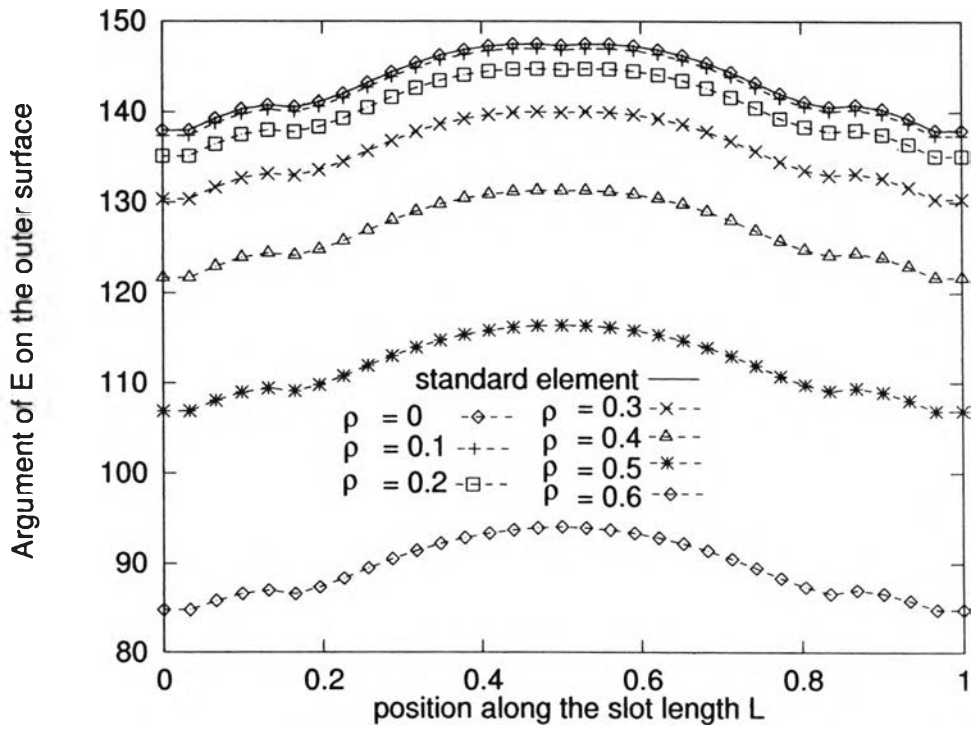

Figure 4.7: The argument of electric field along the outer surface for various number of ρ

The calculation of $\rho = 0$ can be used to verify that the derivation is correct since the zero quadratic parameter means that the characteristic of shape function is linear, so that the result is similar with the standard element. According to the objective of singular element implementation, it should improve the calculation result of electric field distribution around the corners. Therefore, the change of result on other points as shown on those figures is undesirable.

In order to get more explanation of these improper manner, the effect of singular element is analyzed by varying the number of layer for constant number of element per layer and increasing the number of elements with number of layer is kept constant. The results are depicted on Fig. 4.8 to 4.11, respectively.

The variation of the number of layer yields the results as shown in Fig. 4.8 and Fig. 4.9. The graphs show that calculation results of the electric field distribution increase for the larger number of layer but they converge to any values for more than two layers. This convergent number is larger than the calculation with standard element shape function that needs only to layer as shown at the previous subsection. The larger number of layer will increase the number of element on the cavity region and reduce the element size, so that it just change the calculation on the cavity region instead of the surfaces. The formulation of the singular element for the integral on the cavity region changes the nodal value of the singular element. The change of the shape function on the singular element gives more effect to the whole calculation in the low number of element. Therefore, the application of the singular element shape function requires some number of element to get the appropriate result. In this case, the analysis with standard element converges on the two layer so that the number of element is fewer than the required number for singular element shape function.

The graphs on Fig. 4.10 and Fig. 4.11 that depict the result of calculation for various number of element per layer show that the large number of element yields larger result of electric fields distributions. It means that it has more discrepancy with the result with standard element. These improperly changes are possibly caused by the application of the singular element shape function on the moment method calculation where the linear basis function is changed to be a quadratic

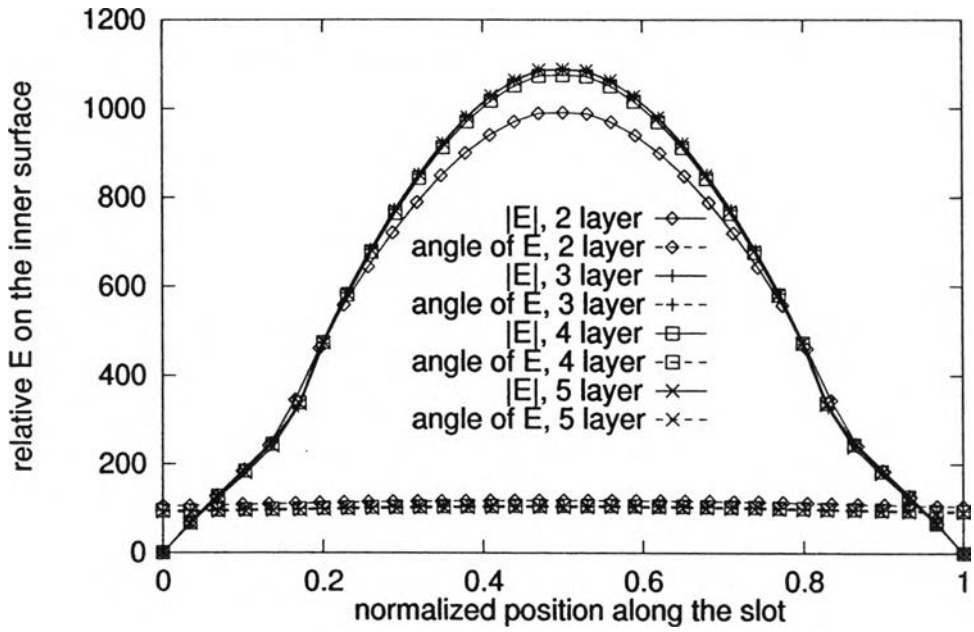

Figure 4.8: The variation of field distribution on the inner surface with various number of layer with $\rho = 0.5$.

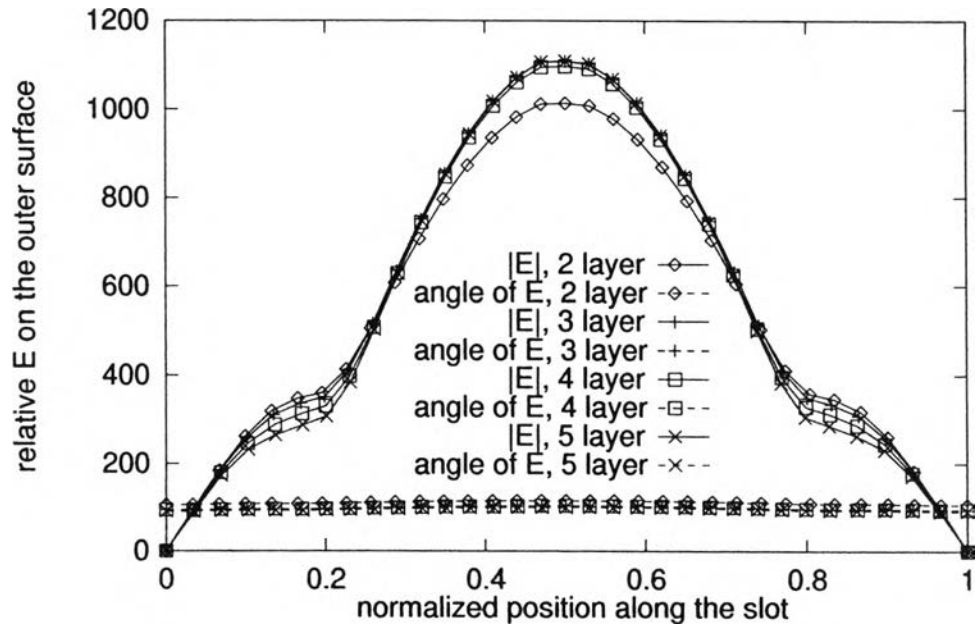

Figure 4.9: The variation of field distribution on the outer surface with various number of layer with $\rho = 0.5$.

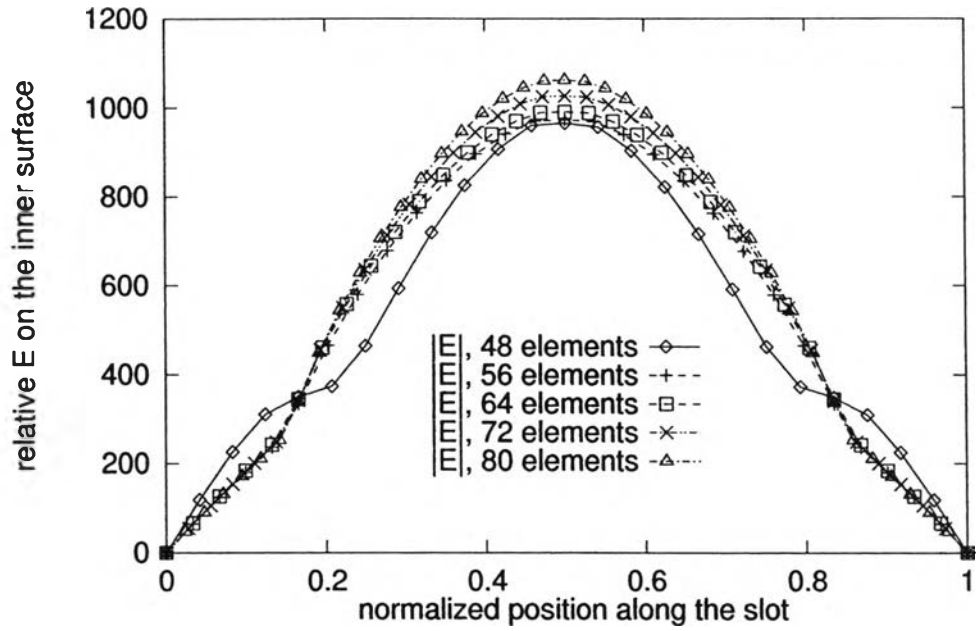

Figure 4.10: The variation of field distribution on the inner surface with various number of elements with $\rho = 0.5$.

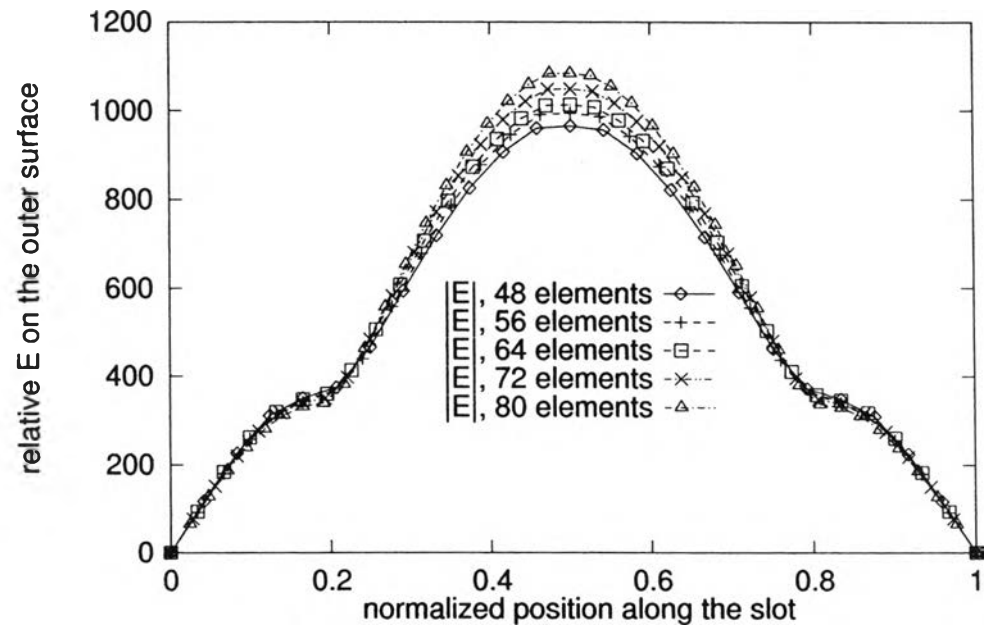

Figure 4.11: The variation of field distribution on the outer surface with various number of elements with $\rho = 0.5$.

form. In the application on pure finite element, the singular shape function just influences the calculation on three nodes of the singular elements, but the change of the basis function on the moment method is also take an effect not only on the nodes of singular element. The fields on the inner surfaces that are induced by the magnetic current sheet are calculated by taking the surface integrals over the observed and source element thus the singular element shape function has an effect if observed field and or source is on the singular element. Therefore, the increment of the surface element number causes more nodes affected by the singular element shape function.

Considering these results, it can be concluded that the singular element shape function is not suitable for the combined finite element and moment methods if the singular point lies on the surface that have to be derived by moment method. In this case the unsuitability is also caused by the low number of layer, but it still converge if the number of layer is increased.

4.4 Calculation of Equivalent Network Parameter

The equivalent network parameter of edge slot is one of the characteristic parameter that can be measured accurately, so that it can be used to verify the numerical analysis as has been done on almost all of previous work.

In order to clarify the result, it is calculated this parameter based on the electric field distribution resulted in this thesis. The conductance and susceptance for some value of slot length are presented on the Fig. 4.12 with its comparison to the other methods.

The graphs of the admittance and susceptance show that the calculation work properly with the results are in between the Jan's work with pure moment method [8] and hybrid FEM/MoM [17]. The resonant length that is calculated from the zero crossing of the susceptance curve yields 0.5168 of wavelength. The admittance properties and the resonant length of the recent work is calculated without singular element shape function. Thus, it should be similar with the Jan's work in

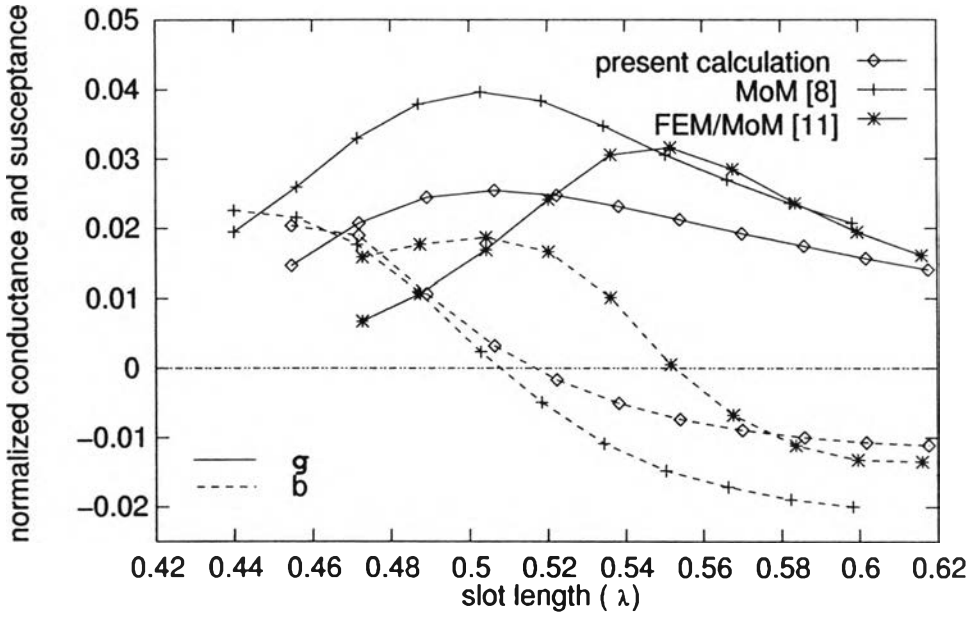

Figure 4.12: Normalized conductance and susceptance of edge slot versus the slot length L and its comparison to some references.

[17]. However, there are some discrepancies on both conductance and susceptance results. It may be caused by inaccuracy of the external Green's function since the information of this function is quite limited in the reference paper.

Nevertheless, the present calculation result of the resonant length is better than the result of real moment method, although the complexity of calculation increases due to the formulation of field in the cavity region that is neglected in the moment method calculations.

Proceeding further, the present calculation is verified to the theoretical reference and measurement data that is provided in [11]. A similar slot as the previous example is analyzed but the depth of cut is fixed $\Delta = 3.5$ mm and various inclination angles. The calculation result of normalized conductance is shown fig. 4.13. The result of calculation and the measurement data on the reference [11] are taken as comparator.

The present calculation obtained lower result that the measurement data. It is possibly caused by any assumptions that is brought into calculation to simplify the analysis. Nevertheless, the curve of current calculation is similar to both theoretical

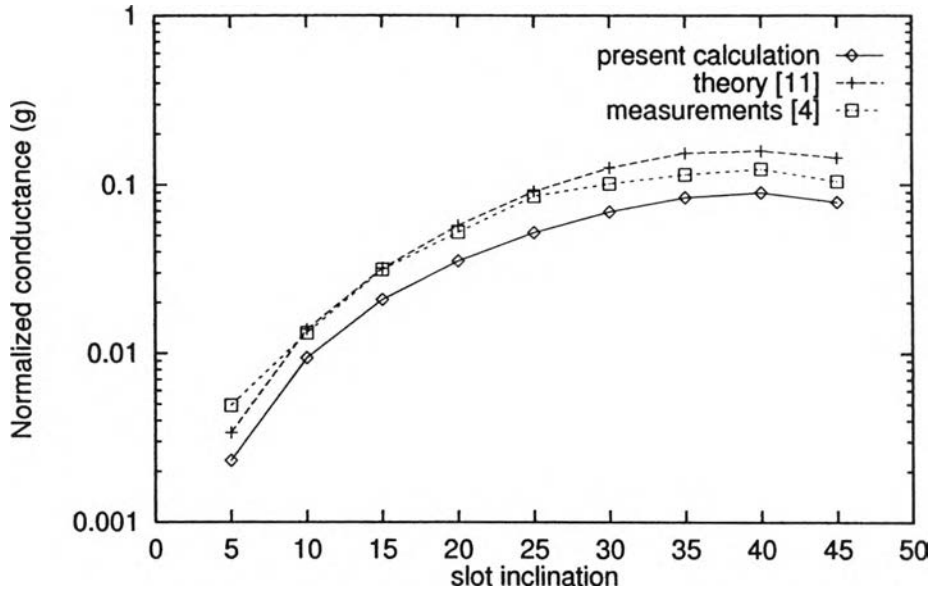

Figure 4.13: Normalized conductance versus slot inclination angle θ and its comparison to other calculation and measurement.

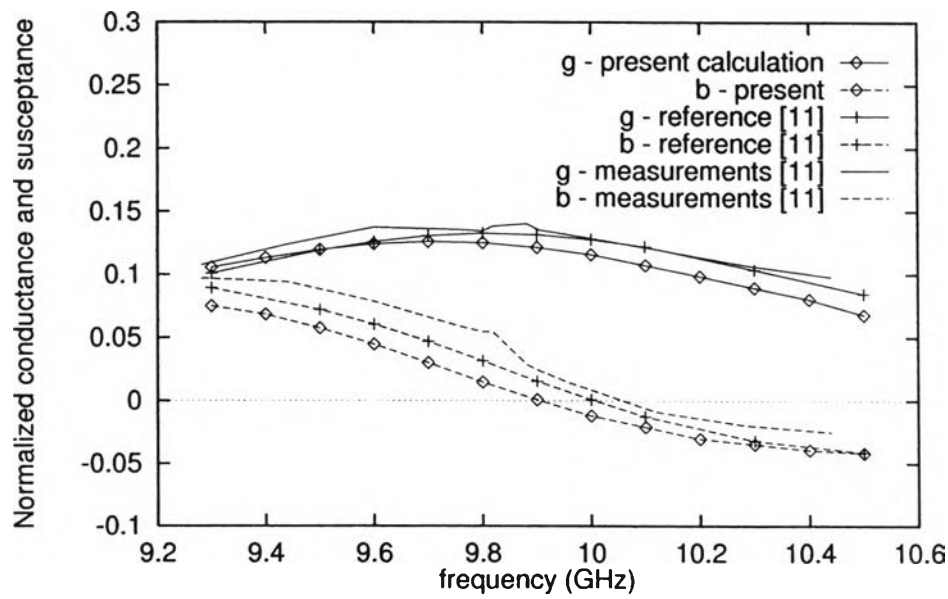

Figure 4.14: Normalized conductance and susceptance of edge slot versus the frequency f and its comparison to other calculation and measurement.

reference and measurement. It shows that the present analysis can work properly and yields correct results.

The next verification is taken by calculating the normalized conductance and susceptance of an edge slot for various frequency. The slot dimension is keep as the previous example, except the depth of cut is $\Delta = 2.60$ mm and inclination angle $\theta = 30°$ to be agree with the published measurement data.

The calculation result is depicted in fig. 4.14. The comparison shows that the present calculation is comparable with the measurement data and theoretical references.

4.5 Radiation Pattern

The radiation pattern of single edge slot is rarely included in the published references, because the complex structure of slot and the presence waveguide corners that can cause some diffractions.

In this thesis, the radiation pattern of an edge slot is approximated by neglecting the effect of the waveguide around the slot. The radiation pattern in the front half space is calculated form the magnetic current sheets along the slot. While the scattered field in backward half space is excluded in the calculation.

The calculation example is taken by calculating the radiation pattern of the edge slot the dimension as mentioned in the first section of this chapter. The radiation pattern are shown on the Fig. 4.15 and Fig. 4.16.

The characteristic of slot antenna is similar with the dipole antenna, but it has polarization in contrary with the slot direction. Fig. 4.15 shows the radiation pattern of edge slot on the H-plane or the $y" - z"$ plane. The pattern has only main lobe with the half-power bandwidth about 40°. The parts of slot that wrap on the broad wall cause the pattern less directed than half wavelength dipole.

Fig. 4.15 shows the pattern on the E-plane or $x" - z"$. The main lobe is wider than on the H-plane, because of the angle of slot inclination.

The radiation pattern of edge slot has low directivity, thus it commonly ap-

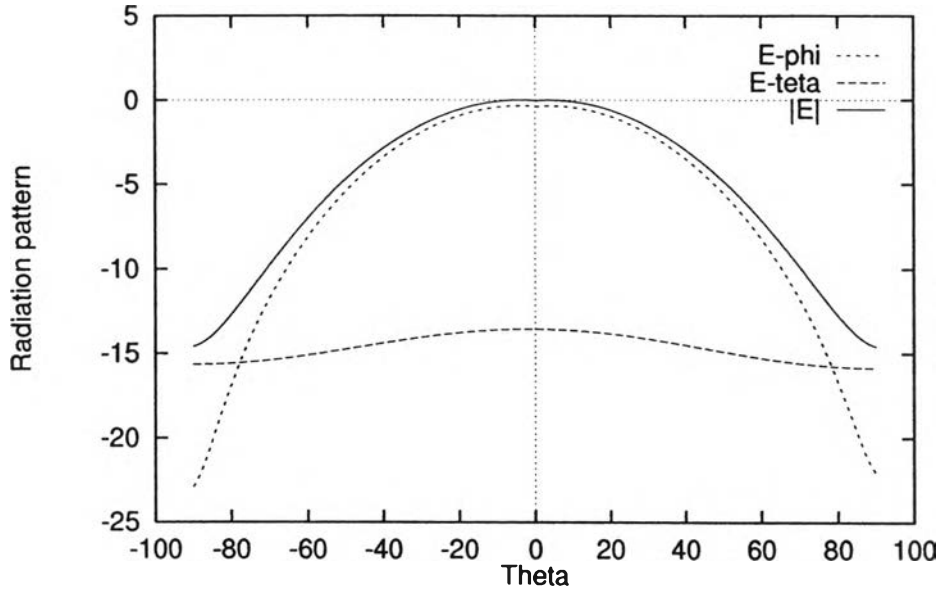

Figure 4.15: Radiation pattern of a single edge slot on the y" $-$ z" plane.

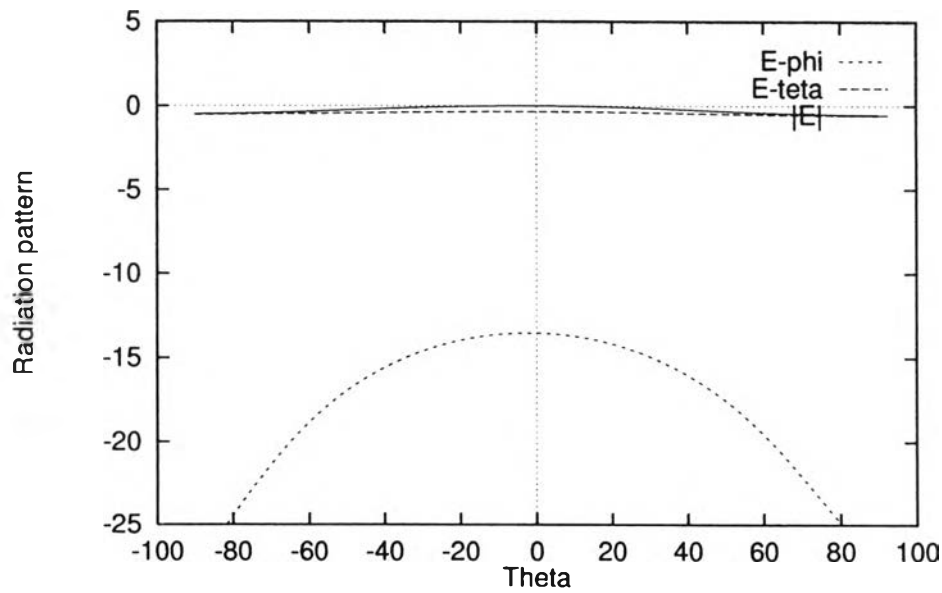

Figure 4.16: Radiation pattern of a single edge slot on the x" $-$ z" plane.

plied as a antenna array. The radiation pattern of edge slot array can be composed from the pattern of single edge slot as done in [14]. In that paper, the electric field distribution along the slot was assumed to be pure sinusoidal. Although it has not been done here, A more precise prediction of pattern must be obtained if thus assumed field distribution is replaced the calculation result.

4.6 Practical Design Considerations

The edge slot antenna as shown in the previous section has low directivity, thus it commonly implemented in array to obtain the desired directivity. The edge slots are milling along one narrow wall of a rectangular waveguide to form a linear array, while the planar array can be composed by placing many similar linear array side by side. The inclination and the length of each slot must be adjusted to optimize the array gain. This section will discuss some design considerations of the edge slot array

The inclination angle of slot causes the phase of the radiated field of the slot is depended on this inclination angle. Fortunately, the phase is changed 180° by inclination on the opposite angle. Therefore, the edge slot array must consists of pair of slot with one has opposite inclination angle to other as shown in Fig. 4.17 so that radiates in phase.

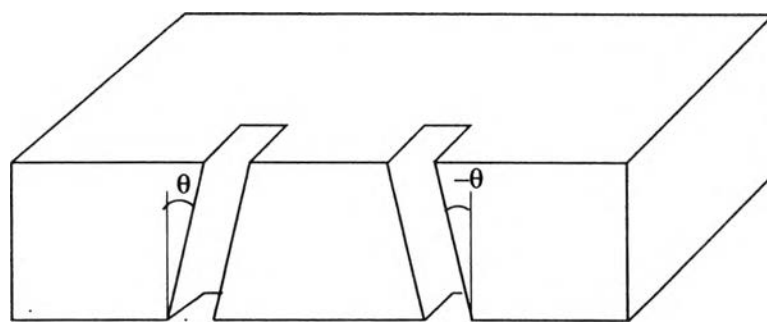

Figure 4.17: A pair of edge slot with the inclination angle is opposite each other.

In order to adjust the inclination angle of each element on the edge slot array, it is modeled a transmission line and shunt loads as shown in Fig. 4.18. The Y_i

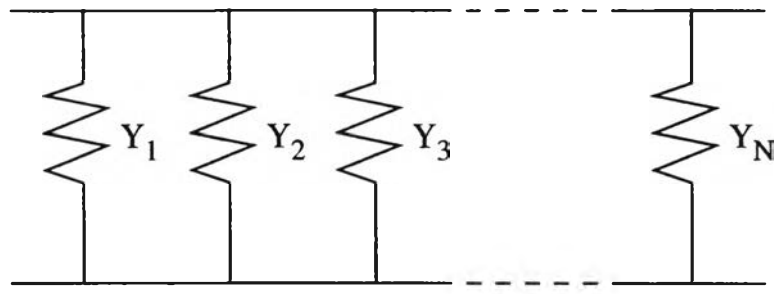

Figure 4.18: Equivalent network parameter of the edge slot array.

are the normalized admittance of the various elements. To get the maximum power radiated from the slot, each slot must be chosen in the resonant length and the total admittance of all elements in the array must equal to one [1]

$$Y = \sum_{i=1}^{N} Y_i = 1 \tag{4.1}$$

where N is the number of element in the array.

Hence the slots are placed closely each other, thus the mutual impedance is also must be accounted in the impedance calculation since the slots couple electromagnetically to each other. Therefore, the admittance of each array component consists of the self-admittance of edge slot and mutual admittance.

$$Y_i = Y_{ii} + \sum_{j=1}^{N}{}' Y_{ij} \tag{4.2}$$

where Y_{ii} is the self-admittance, Y_{ij} is the mutual admittance, and $\sum'$ denotes the summation with the term $i = j$ is excluded.

Assuming that the excitation wave inside the waveguide does not attenuate along the waveguide, the admittance of each element can be obtained from the resonant admittance of a single edge slot as calculating in this thesis. The mutual admittance that is not derived in this work can be obtained on other references such as in [12] and [14]. It is worth noting that the array element spacing has an effect to the mutual admittance, so that it must be chosen by considering its mutual coupling and the provided space for the edge slot array. The optimum condition in (4.1) can be approximated by adjusting the inclination angle of each element. The depth

of slot cut for each element is calculated from the resonant length according to its inclination angle.

The radiation pattern of the edge slot array can be predicted from the electric field distribution of each element. If the result of radiation pattern is less then the desired directivity, it can be improved by increasing the number of array element.

In this procedure, the practical design of the edge slot array needs the accurate information of the admittance properties of a single edge slot to get the optimum array design. Although this procedure has not been done in this thesis due to the time constraint, the thesis contributes to provide the numerical calculation of admittance parameters.